Articles in PresS. J Neurophysiol (April 20, 2016). doi:10.1152/jn.00019.2016

Accommodation to hyperpolarization of human axons assessed in the frequency domain

James Howells[1], Hugh Bostock[2] and David Burke[3]

[1]*Brain & Mind Centre, The University of Sydney, Sydney, Australia*

[2]*Sobell Department of Motor Neuroscience and Movement Disorders, Institute of Neurology, University College London, Queen Square, London, UK*

[3]*Royal Prince Alfred Hospital and The University of Sydney, Sydney, Australia*

Corresponding Author:

James Howells

Level 2, Medical Foundation Building

The University of Sydney

92-94 Parramatta Rd, Camperdown 2050, N.S.W., Australia.

Email: james.howells@sydney.edu.au

Running title: *Low-frequency resonance in human axons*

Keywords: *axonal excitability, frequency domain, resonance, motor axons, sensory axons, HCN channels, I_h, mathematical modelling*

Number of pages:45

Number of figures: *9*

Number of tables: *2*

Word count (excluding title page, references, tables, figure legends and appendix):

6582

Abstract

Human axons *in vivo* were subjected to subthreshold currents with a threshold-"ZAP" profile (Impedance [Z] Amplitude Profile) to allow the use of frequency domain techniques to determine the propensity for resonant behavior, and to clarify the relative contributions of different ion channels to their low-frequency responsiveness. Twenty-four studies were performed on the motor and sensory axons of the median nerve in 6 subjects. The response to oscillatory currents was tested between 'DC' and 16 Hz. A resonant peak at ~2 to 2.5 Hz was found in the response of hyperpolarized axons, but there was only a small broad response in axons at resting membrane potential (RMP). A mathematical model of axonal excitability developed using DC pulses provided a good fit to the frequency response for human axons, and indicated that the hyperpolarization-activated current I_h, and the slow potassium current I_{Ks} are principally responsible for the resonance. However the results indicate that if axons are hyperpolarized more than -60% of resting threshold, the only conductances that are appreciably active are I_h and the leak conductance – i.e., that the activity of these conductances can be studied *in vivo* virtually in isolation at hyperpolarized membrane potentials. Given that the leak conductance dampens resonance it is suggested that the -60% hyperpolarization used here is optimal for I_h. As expected differences between the frequency responses of motor and sensory axons were present and best explained by reduced G_{Ks}, up-modulation of I_h and increased persistent Na^+ current, I_{NaP} (due to depolarization of RMP) in sensory axons.

New and Noteworthy

The low-frequency response of human axons was studied *in vivo* using a novel application of frequency-domain and threshold-tracking techniques.

Studying the response to subthreshold oscillatory input currents at different membrane potentials allows the separation of relative ion channel contributions to axonal excitability based upon their voltage dependence and gating kinetics.

At hyperpolarized membrane potentials, hyperpolarization-activated conductances which flow through HCN channels are responsible for low-frequency resonance in human axons which is modulated by leak conductances.

Abbreviations

FFT, Fast Fourier Transform; f_{max}, frequency corresponding to the maximal 'threshold impedance' (Z_{max}); $G_{Lk,}$ leak conductance; G_{Ks}, slow-potassium conductance; G_H, hyperpolarization-activated conductance; HCN, hyperpolarization-activated cyclic nucleotide-gated channels; I_h, hyperpolarization-activated cation current; I_{Ks}, slow-potassium current; I_{NaP}, persistent Na^+ current; K_f, fast potassium; K_s, slow potassium; RMP, resting membrane potential; SNR, signal to noise ratio; ZAP, Impedance[Z] Amplitude Profile; '$Z_{threshold}$', threshold analog of impedance;.$Z_{0.5}$, magnitude of 'threshold impedance' at 0.5 Hz; Z_{max}, maximal magnitude of 'threshold impedance'

Introduction

In humans, studies of the excitability of human peripheral nerve axons have been undertaken using threshold-tracking techniques and have provided insight into the biophysical determinants of excitability in health and disease (Bostock et al. 1998;

Burke et al. 2001; Kiernan et al. 2000; Krishnan et al. 2009). Traditionally conditioning stimuli have been square-wave currents, either subthreshold and long-lasting, or brief and at or above threshold. The contribution of the inwardly rectifying current, I_h, is apparent in the accommodation to hyperpolarizing changes in membrane potential, but this requires long and strong hyperpolarization before it can be appreciated fully (Howells et al. 2013; Howells et al. 2012; Tomlinson et al. 2010).

The accommodation to hyperpolarization is mediated by several conductances. For example, over the voltage range in which they overlap, changes in the rectifying conductances G_{Ks} (slow potassium) and G_H (hyperpolarization-activated) have synergistic effects: hyperpolarization of the membrane potential leads to a lessening of the hyperpolarizing conductance G_{Ks} and an increase in the depolarizing conductance G_H. Both changes act to limit the hyperpolarization.

The disentanglement of the relative contributions has traditionally focussed on the overall picture of excitability, with the effects of G_{Ks} also present in the accommodation to depolarizing currents and in the late subexcitable period following an action potential (Kiernan et al. 2000). To complicate the picture further, it is difficult to separate these slowly rectifying currents from the leak conductance (G_{Lk}), which is independent of membrane potential. Despite these issues, this 'whole-of-excitability' approach has allowed the development of mathematical models which have been successful in describing the biophysical basis of axonal excitability in health and a variety of disease processes (Howells et al. 2012; Krishnan et al. 2009; Lin et al. 2006).

The use of frequency as a probe of structure and function is well established. Cole and Curtis (1936) described the impedance of nerve and muscle in terms of an equivalent electrical circuit consisting of a parallel resistance and capacitance, and this

92 model was later extended on functional grounds to include an inductive element to
93 explain the rectifying properties of axon membranes (Cole 1941; Cole and Baker 1941).
94 Puil and colleagues (1986) introduced a frequency probe, which they called the ZAP
95 (Impedance[**Z**] **A**mplitude **P**rofile) as an efficient means to probe the passive and active
96 properties of trigeminal root ganglion neurons in guinea pigs. The ZAP is essentially a
97 small amplitude sinewave current whose instantaneous frequency is continuously
98 increased from start to end. The response voltage to such a current provides a frequency
99 response profile within a single sweep, and this depends on the particular membrane
100 structure and the composition and state of the ion channels present in the membrane
101 (Hutcheon and Yarom 2000; Llinás 1988). To date, studies have focussed on the low-
102 frequency subthreshold resonance that underlies θ-rhythms in central neurons (Hu et al.
103 2009; Hu et al. 2002; Hutcheon et al. 1996; Pike et al. 2000; Wang et al. 2006;
104 Zemankovics et al. 2010). Hu and colleagues (2002) found that θ-resonances occurred
105 at hyperpolarized and depolarized membrane potentials, mediated by HCN and K_s
106 channels, respectively, and they termed these H- and M-resonances. No studies have
107 been performed on axons, and the techniques have not been applied previously to
108 human tissue *in vivo*.
109 Experiments *in vivo* on human subjects inevitably rely on indirect techniques,
110 and conclusions are more convincing when supported by different approaches. In the
111 present study a new protocol was developed to assess the suitability of using threshold
112 tracking techniques to investigate the responses of human axons in the frequency
113 domain. Motor and sensory axons of the median nerve were subjected to subthreshold
114 oscillatory currents, both at resting and hyperpolarized membrane potentials. The
115 results were interpreted with the help of a previously described model of axonal

excitability (Howells et al. 2012), and used to re-examine the nature of the differences between motor and sensory axons.

Materials and Methods

Twenty-four experiments were performed on six subjects. The experiments each lasted ~ 2 hours, and they were carried out on separate days. The subjects provided written consent prior to the study, which was approved by the Human Research Ethics Committee of The University of Sydney and conformed to the *Declaration of Helsinki*.

All excitability measurements were made using the QTRAC threshold-tracking software (© Institute of Neurology, University College London, UK). The ZAP protocol was developed in QtracS, and synchronized the delivery of the stimulus command signals with the acquisition of the compound action potentials via a data acquisition system (PCI-6221, National Instruments, Austin, TX). The compound action potentials were amplified using a purpose-built low-noise amplifier, and mains frequency noise was removed using a Humbug noise eliminator (Quest Scientific, Vancouver) before being digitized by the data acquisition system.

The ZAP protocol was applied to motor and sensory axons of the median nerve at the wrist. The pulse protocols in the present study required the delivery of long subthreshold pulses, which necessitated special stimulation measures to prevent polarization of electrodes and long-term polarization of resting membrane potential (RMP). Skin impedance at the stimulus sites was reduced using abrasive tape (Red Dot Trace Prep, 3M), followed by cleaning with an alcohol swab. The optimal cathode location (at the wrist) was sought using a saline-soaked gauze-covered electrode before

applying the final stimulation cathode. Disposable self-adhesive Ag/AgCl electrodes (Unilect 1010M) were used for stimulation, ground and EMG recording electrodes. The anode was remote from the median nerve, approximately 10 cm proximal to the cathode and toward the radial edge of the forearm. Compound muscle action potentials (CMAPs) were recorded from the thenar eminence, with the reference electrode on the distal phalanx of digit 1. Self-adhesive Ag/AgCl ring electrodes (RE-D, Electrode Store) were used for recording compound sensory action potentials (CSAPs) of the index finger, with the active electrode on the proximal phalanx of digit 2, and the reference 4 cm distal (Eduardo and Burke 1988). The ground electrode was placed on the dorsum of the hand for both motor and sensory recordings. Skin temperature was monitored using a thermistor (YSI-409B) located close to the site of stimulation, and recordings began when the temperature was stable and above 32°C.

'Threshold ZAP' protocol

A threshold analog of the ZAP (impedance [**Z**] **a**mplitude **p**rofile) technique introduced by Puil and colleagues (1986) was developed for these experiments to enable the *in vivo* study of the frequency response of human axons. This protocol utilizes the empirical observation of Bostock and Baker (1988) that the excitability changes to subthreshold polarization (threshold electrotonus) mirror the underlying electrotonic changes in membrane potential. The suitability of this approach was first assessed by testing the linearity of the correlation between membrane potential and excitability in a mathematical model of the human motor axon (see first section of Results).

The threshold to various conditioning currents was tested using a 1-ms test pulse, with the aim of minimizing test stimulus intensities, conditioning currents, and

therefore pulse energies. As in all threshold-tracking studies a stimulus-response relationship was recorded and then used to establish the current required to produce the target CMAP or CSAP (50% of maximum in this instance) that was used for the rest of the protocol. This current is referred to as the 'threshold' for the target potential.

The 'threshold ZAP' protocol measured the response to a linear "chirp" signal (or swept sinewave), whose frequency was increased linearly from DC to 16 Hz over 4 s and 16 s for human and model studies, respectively. The amplitude of the ZAP was a fixed fraction of the unconditioned (control) threshold . It is described by the equation:

$$ZAP(t) = a * \sin\left(\pi * \frac{f_{max}}{T} * t^2\right)$$

where, a is the amplitude of the chirp , f_{max} is the maximal frequency (in Hz; 16 in the present study), T is the length of the ZAP stimulus (in seconds) and t is time (in seconds).

The low-frequency range employed in the present study is likely to exclude a significant tissue filtering contribution to the frequency dependence, because extra-neural impedance can be regarded as essentially resistive at these frequencies (Gabriel 1996; Logothetis et al. 2007).

To examine the role of I_h in the frequency response of human axons, the ZAP signal was superimposed on a hyperpolarizing current of 60% of the control threshold (i.e. -60% of the current required to produce a 50% CMAP or CSAP). This level was chosen as the strongest level of hyperpolarization achievable without unintended stimulation of axons by the supposedly subthreshold current, while still likely to be strong enough to exclude significant involvement of K_s channels, which might

otherwise contribute to low-frequency attenuation (Howells et al. 2012). Subsequent findings supported this choice.

The ZAP started 200 ms after the onset of the constant polarization. This delay was sufficiently long to be after the majority of the 'fast' accommodation and was chosen to correspond to the time delay used in conventional I/V measurements, from which the threshold conductance is estimated (Kiernan et al. 2000).

The underlying threshold electrotonus in response to the 60% hyperpolarization was recorded in detail during the period of 'fast' accommodation and then more slowly at time points corresponding to every 500 ms during the ZAP current.

The entire protocol was balanced to prevent polarization of the electrodes and resting membrane potential. On the sweep following every conditioning stimulus an 'anti-stimulus' was delivered which was equal in magnitude but opposite in polarity.

For the experimental studies on human subjects, the stimulus threshold was sampled 128 times every 31.25 ms (32 Hz) during the 4,000-ms ZAP current, to facilitate analysis using a Fast Fourier Transform (FFT).

The QtracS protocol automatically advanced the test condition (test stimulus location within ZAP or threshold electrotonus) when 2 acceptable measurements were made. A measurement was deemed acceptable if the response was within 5% of the target, or if the test threshold resulted in responses which bracketed the target.

Analysis of frequency-response curves

In the time domain, the threshold was tracked 128 times at evenly-spaced conditioning test intervals of 31.25 ms throughout the ZAP. As in the calculation of threshold electrotonus, the excitability at each time point was calculated as the normalized threshold reduction:

$$Excitability\ (threshold\ reduction, \%) = \frac{threshold_{control} - threshold_{ZAP}}{threshold_{control}}$$

The analysis of frequency response was performed offline, using a custom script written in Matlab (R2012a). For the recordings made with polarization, the effects of threshold electrotonus were first subtracted from the ZAP response. Any residual trend in the ZAP response was removed prior to conversion to the frequency domain using a FFT.

In a manner analogous to that introduced by Puil and colleagues (1986), a new measure, $'Z_{threshold}'$ relating the response (excitability) to input waveforms, was constructed as follows:

$$'Z'_{threshold} = \frac{FFT(Excitability)}{FFT(input)}$$

$'Z_{threshold}'$ is a complex-valued data set with real (resistive) and imaginary (reactive) components, and is the threshold analog of impedance, much as 'threshold electrotonus' results from and is related to electrotonic changes in membrane potential. The phase of the 'threshold impedance' ($\phi_{threshold}$) represents the difference in phase between the threshold response and input current waveforms.

The frequency response curve was constructed by plotting the magnitude of 'threshold impedance' ($|'Z_{threshold}'|$) versus frequency, from which the spectral parameters: $Z_{0.5}$, Z_{max}, f_{max}, Q were calculated. Using the definitions from earlier studies (Hutcheon et al. 1996; Orio et al. 2009; Zemankovics et al. 2010): $Z_{0.5}$ is defined as the impedance at 0.5 Hz; Z_{max} and f_{max} are the maximal impedance and corresponding frequency; and Q the ratio of Z_{max} to $Z_{0.5}$.

The suitability of this approach was examined in a mathematical model by comparing the electrical impedance (calculated using membrane potential) to the new

measure of 'threshold impedance' (see Results). The results based on ZAP currents were then compared to measurements based on pure single-frequency sinusoidal input currents.

Modelling

A mathematical model of the excitability of human motor and sensory axons, based on the motor axon model of Bostock et al. (1991b) and developed in Howells et al. (2012), was used to examine the basis of the low-frequency response of human motor and sensory axons. This model consists of two compartments, a node and an internode linked by the 'Barrett-Barrett' paranodal pathways through and under the myelin sheath (Barrett and Barrett 1982). Na^+ currents (transient and persistent), slow and fast K^+ currents, leak and pump currents along with the internodally located hyperpolarization-activated conductance I_h are the key determinants of the excitability of large myelinated fibres and are represented in this model. The equations and parameters describing this model are listed in full in the Appendix.

The models were subjected to the same ZAP protocol, with the exception that the target threshold was defined as the minimal threshold to generate an action potential.

If alterations in model parameters resulted in much larger oscillations of excitability, the ZAP amplitude was decreased to maintain linearity of the response.

Results

Linearization of the ZAP protocol

The amplitude of the ZAP was chosen to be sufficiently large to give a good signal-to-noise ratio, but small enough to maintain linearity of the response (Koch 1984). The linearity of the underlying membrane potential response was assessed using

a 10% ZAP superimposed on a hyperpolarization of 60% (of the control threshold; Fig 1a) using the mathematical model in Howells et al. (2012). The maximal peak-to-peak membrane potential deflection was 9.6 mV (blue trace in Fig 1b) which is well below the 20-mV criterion for linearity established by Hutcheon and colleagues (1996).

An additional measure of the nonlinearity of the response was made by averaging the response to this initially downward-going ZAP and its mirror (i.e. an initially upward-going ZAP) and subtracting the electrotonic response to the DC polarization. The peak nonlinearity calculated this way was 0.1 mV and occurred between the peak deflections at a time corresponding to 1.9 Hz.

Linearity of excitability as an output measure

In a bid to assess the suitability of threshold to a linear systems formulation, a ZAP input stimulus was applied to the motor axon model (Fig. 1a), and both the resultant membrane potential (Fig. 1b) and excitability (Fig. 1c) were calculated. For both of these input signals (RMP and -60%), excitability was linearly correlated to membrane potential ($R^2 = 0.9998$). Electrical impedance was transformed to the frequency domain and calculated in the usual way using the ratio: FFT(V)/FFT(I), and the magnitude and phase are shown in Fig 1e,h. By analogy with the term 'threshold electrotonus' used for the threshold analog of membrane potential, the proposed measure $'Z_{threshold}'$ was calculated as FFT(excitability)/FFT(I). Its magnitude and phase are shown in Fig 1f,i. Under the present experimental conditions there was a tight correlation in the modelled data between $'Z_{threshold}'$ and $Z_{electrical}$ as shown in Fig. 2. At hyperpolarized membrane potentials the magnitude and phase for both measures were linearly correlated from DC to 16 Hz ($R^2 = 0.9997$, 0.997, respectively; Fig 2b,c green to blue data). At RMP the magnitude and phase were also correlated ($R^2 = 0.90$,

278 0.98, respectively; yellow to red data), though at low frequencies (< ~2 Hz; yellow data
279 points), the magnitude of $'Z_{threshold}'$ appears to be underestimated using the ZAP
280 protocol.

281 For comparison, the electrical impedance was calculated in response to single
282 frequency sinusoids at selected frequencies and the magnitude and phase are plotted in
283 Fig 1d,g. A linear regression of the magnitude and phase of $Z_{electrical}$ calculated this
284 way versus the data derived using a ZAP stimulus gave good correlations with R^2
285 values of 0.95 and 0.98, respectively.

286 ## *In vivo* measurement of the frequency response of human axons

287 Excitability (measured as reduction in threshold) is an effective *in vivo* measure
288 of the response to an input current. However, unlike studies of resonance and the
289 frequency preference of membrane potential in neurons (Hu et al. 2002; Hutcheon et al.
290 1996; Orio et al. 2009; Puil et al. 1986; Puil et al. 1988; Puil et al. 1994; Wang et al.
291 2006; Zemankovics et al. 2010), the time taken to record each data point with threshold
292 tracking is much greater. This imposes a limit on both the frequency resolution and the
293 maximal frequency recorded. The ZAP recordings for the modelled data involve
294 polarizing currents longer than 16 s, with sampling of at least 512 points. Such
295 measurements are impracticable in human subjects, as they would result in unacceptably
296 long polarizing currents and recordings which could take up to 32 hours. A
297 compromise was made to record 128 time points over a 4-s ZAP, and a comparison of
298 these 4-s vs 16-s recordings is shown for the model in Fig. 3. Apart from a loss of low-
299 frequency phase resolution (<1Hz for -60%, and < 2 Hz for RMP) and some folding
300 back of higher frequencies at frequencies >~8Hz, acceptable recordings could be

recorded in a fraction of the time. The regression lines for amplitude and phase were close to the line of identity (see legend to Fig. 3).

Balancing the stimulation protocol led to a near doubling of the recording time, but prevented polarization of the electrodes and damage to the skin. An average of 1507 stimulus sweeps were delivered [range 1057 to 2351] for each recording, resulting in ~12 sweeps / sample point (this includes balance, control stimulus and stimulus / response sweeps), resulting in a 'cost' for each data point of ~53 seconds.

Most experiments were complete within 2 hours, and in recordings with good signal-to-noise ratios the tracking was faster and the studies were complete within 1.5 hours. Even though the protocol was balanced and should not have any long-term effect on axonal excitability, the 24 recordings were made on different days.

The resonance protocol was well tolerated by all subjects, and Fig. 4 shows that despite these challenges a resonant peak was clearly visible in all recordings, particularly during hyperpolarization (shown in blue).

Frequency-response curves

The individual responses to the unpolarized ZAP current are shown in Figure 4 (top row, red traces), and their near perfect superimposition shows little variation between subjects in both motor and sensory axons. For each time point the maximal difference between any two pairs of responses at RMP was, on average, 5.5% and 6.1% for the motor and sensory axons, respectively. As is usual for the response to hyperpolarization (see Howells et al. 2012; Tomlinson et al. 2010), there was considerable variability between subjects in the 'threshold electrotonic' responses, -180%(range: -222 to -144%) for motor axons and -135% (range: -154 to -113%) for sensory axons The mean 'threshold electrotonic responses were significantly different

between motor and sensory axons (p=.006). However after subtraction of the electrotonic response to 60% hyperpolarization, the average maximal difference between any two responses during hyperpolarization was 11.4% and 12.7% for the motor and sensory axons, respectively. The lesser hyperpolarization in sensory axons and the variability of the threshold electrotonic baseline confirm earlier findings (Bostock et al. 1994; Howells et al. 2013; Howells et al. 2012; Lin et al. 2002; Tomlinson et al. 2010). This enhanced variability with hyperpolarization probably contributes to the greater variability of the resonant peak in the hyperpolarized axons (Fig. 4 middle row). The peak impedance magnitude (Z_{max}, listed in Table 1) was inversely and linearly correlated to the mean threshold electrotonic level for both motor and sensory axons with R^2 values of 0.83 and 0.89 respectively.

The 'threshold impedance' across the studied frequency range was greater in motor axons than sensory for both RMP ($p<.009$) and hyperpolarization ($p<0.01$).

In hyperpolarized motor and sensory axons there was a resonant peak in all subjects, though the 'noise' between adjacent measurements in the frequency domain also contributed to the variation in the derived spectral parameters. To mitigate this point-to-point variation, the spectral parameters were also calculated after first fitting a Pearson Type IV function to the data (Orio et al. 2009). This function fitted the frequency-response curves well for the hyperpolarized data (Table 1) and, on the whole, reduced the variation in the parameters (see bracketed values in Table 1).

The resonant responses to oscillatory inputs of both motor and sensory axons were greater at hyperpolarized membrane potentials than at RMP, as evidenced by the greater Z_{max} and Q-values (Fig. 4 and Table 1) and were comparable to studies of neuronal cells in which the frequency response has been shown to have a voltage

dependence (Gutfreund et al. 1995; Hu et al. 2002; Hutcheon et al. 1996; Wang et al. 2006). The resonant frequency for the hyperpolarized axons occurred at 2.1 and 2.5 Hz for the motor and sensory axons respectively.

.

Computational Model

Assessment of the mathematical models in the frequency domain

The recorded responses to the ZAP protocol were then compared to the responses of the mathematical models in Howells et al. (2012), derived using DC conditioning stimuli (Fig. 5). The motor and sensory models provided good fits to the mean changes in excitability in response to the ZAP protocol measured at RMP (Fig. 5: compare upper red and black traces in the top row; with correlation coefficients of 0.99 and 0.95 for motor and sensory axons, respectively). With a 60% hyperpolarization correlations were similarly tight (R^2 = 0.98, 0.96), but the motor axon model had a slightly more hyperpolarized baseline than the group data (motor model, -204%; motor data -180), and the sensory axon model slightly depolarized when compared to the sensory group data (sensory model, -126%; sensory data, -135. These shifts are small and could result from differences in activation of I_h between subjects (Howells et al. 2013; Howells et al. 2012; Tomlinson et al. 2010) and/or variation in extracellular K^+ levels (Boërio et al. 2014).

In the frequency domain, the modelled excitability data showed the same key features of resonance as the group data, both qualitatively and quantitatively, namely a voltage-dependent resonant peak that was greater in motor axons than sensory. The summary statistics of the modelled spectral data are given in Table 2.

The voltage dependence of the frequency response

373 Given the good fit of the modelled data to the experimental data, the voltage
374 dependence of the frequency response was modelled for motor axons at RMP (0%) and
375 with background hyperpolarizations of 30, 60 and 90% of the control threshold (Fig. 6).
376 As described in the methods, the majority of the early phases of threshold
377 electrotonus were complete by the start of the ZAP protocol (200 ms after the onset of
378 the hyperpolarization; Fig. 6a). The resonant response grew with hyperpolarization, as
379 previously reported for various neurons in guinea pigs and rats (Gutfreund et al. 1995;
380 Hutcheon et al. 1996; Wang et al. 2006), to a peak which was maximal in the present
381 study with a 60% hyperpolarization (Fig. 6b,c).

382 **The contribution of slowly rectifying conductances to the frequency response**

383 The mathematical model was used to explore the role of key ion channels to the
384 observed resonance in human motor axons (Fig. 7). The frequency response and its
385 voltage-dependence is reflected in, and indeed driven by, the interaction between I_{Ks},
386 I_{NaP} , I_h and I_{Lk}.

387 ***At RMP*** the response to the ZAP input was dominated by I_{Ks} in a frequency-
388 dependent manner, with the greatest response at low frequencies and a gradual decline
389 in amplitude with increasing frequency (see green in the left column of Fig. 7).
390 Unsurprisingly I_h did not contribute significantly to the frequency response at rest.

391 ***With 60% hyperpolarization*** slow K^+ channels were largely deactivated. Less
392 than 1% of K_s channels were open, and because membrane potential was below the
393 equilibrium potential for K^+, these channels passed a small *depolarizing* current. In
394 contrast, roughly one third of HCN channels were activated, with I_h opposing low-
395 frequency inputs preferentially providing the mechanism for resonance in
396 hyperpolarized axons.

Conductances that alter the magnitude of the frequency response

The influence of the leak conductance (G_{Lk}) was smaller at RMP (grey curves in left column of Fig. 7) and increased with polarization, consistent with an ohmic conductance modelled with a reversal potential near resting membrane potential. The effect of G_{Lk} can be seen purely in terms of its effect on the input conductance, and its ability to 'leak' current across the membrane. G_{Lk} opposed fluctuations in membrane potential independent of frequency, and therefore progressively suppressed resonance with increasing polarization. This implies that the 60% hyperpolarization used here may be optimal for studying I_h. At 60% hyperpolarization the magnitude of I_{Lk} is comparable to that of I_h (compare grey and red curves in right column of Fig. 7), but importantly it varies in phase with and proportional to changes in membrane potential.

In contrast an increase in the fraction of sodium channels operating in a persistent mode *amplifies* resonance at RMP, and its effect on the frequency-response curves *diminishes* rapidly with hyperpolarization, as seen in Figure 7.

Sensitivity of frequency response to key currents

A sensitivity analysis was performed on each of the key conductances in the model of a motor axon. For each conductance, the effect of complete removal of the conductance and a doubling of the conductance were compared to the normal level in the unaltered model. The ZAP measurements were then made at the same membrane potentials (RMP and -60%) as in the unaltered model.

The frequency response at RMP, was sensitive to a reduction in G_{Ks} (compare dotted and thin red curves in Fig 8b) with no appreciable contribution by G_H. As previously discussed, G_{Lk} attenuates and P_{NaP} amplifies resonance at RMP (compare red curves in Fig 8c and d).

With 60% hyperpolarization, P_{NaP} and G_{Ks} have a negligible effect on $Z_{electrical}$, with G_H responsible for the resonance which is sensitively modulated by leak conductances (removal of G_{Lk} increases Z_{max} by 166% and doubling G_{Lk} decreases Z_{max} by 38%).

Do sensory axons behave as relatively depolarized motor axons?

The model was used to assess the possibility that differences in the frequency response of motor and sensory axons can be attributed to differences in their resting membrane potentials. Figure 9 shows that the discrepancy in response between the motor and sensory models is reduced by 94.9% (RMP) and 99.7% (60% hyperpolarization) when the motor model is depolarized by 3-mV. However, this degree of depolarization reduced the discrepancy in the frequency response curves by 97% (RMP) and 29.2% (60% hyperpolarization) implying that there are probably other differences between sensory and motor axons.

Discussion

The present study has examined the low-frequency response of human axons *in vivo* using a novel application of frequency-domain and threshold-tracking techniques. Studying the response to subthreshold oscillatory input currents at different membrane potentials allows the separation of the ion channel contributions to axonal excitability based upon their voltage dependence and gating kinetics. We provide evidence that changes in excitability reflect changes in membrane potential, at least under the conditions of the present studies. The findings using the ZAP protocol and their compatibility with studies that have relied on square-wave DC pulses validates the present approach as a technique for studying ion channel function in human axons

444 *in vivo*. In the absence of evidence for K_{IR} channels in myelinated axons of the
445 peripheral nervous system, we attribute inward rectification to HCN channels in the
446 following discussion.

447 Traditional threshold-tracking techniques probe the slowly-gated inwardly-
448 rectifying conductance G_H using long-lasting hyperpolarizing square-wave conditioning
449 currents, but these conditioning stimuli do not easily separate out the contributions of
450 voltage-dependent (G_{Ks}), and ohmic (G_{Lk}) conductances. This new protocol attempts to
451 address these limitations by adding frequency-domain techniques to further distinguish
452 these conductances.

453 There are a number of ways in which channel activity could be modulated
454 through intra- or extra-cellular mechanisms affecting the gating or changes in channel
455 expression. The present study focusses on overall channel activity not the mechanisms
456 underlying any differences in activity.

457 The mathematical models of the behavior of human sensory and motor axons
458 described in Howells et al. (2012) were subjected to this new frequency probe, and
459 adequately describe the response to oscillatory inputs. This provides independent
460 validation of these models, which were then used to examine the factors responsible for
461 generating and amplifying (or attenuating) resonance in human axons.

462 One limitation of this technique as implemented in the current study is the time
463 taken for an entire recording. Depending on the application, there are several strategies
464 that could be employed in future studies. The standard FFT approach requires a
465 uniform spacing of data points collected in the time domain, but sampling at high
466 frequencies during the low-frequency component of the ZAP is costly. Non-uniform
467 sampling techniques could be employed to speed up the protocol. Reducing the

sampling interval to 62.5 ms, would limit the upper frequency studied to 8 Hz, but would nearly halve the recording time. Reducing the sweep length would also have a major impact on the recording time but unfortunately would also reduce the resolution in the frequency domain. Another approach may be to measure pure sinusoids at desired frequencies only. A careful analysis of the minimum number of data points required to resolve amplitude and phase of the threshold response would need to be performed, but a rough estimate based on an angular resolution of 45° would require 8 data points / frequency studied.

Excitability as a measure of membrane potential

Direct comparisons of the threshold and electrotonic responses in the same axons are difficult and not possible in human axons *in vivo*. The present study has compared these responses in a model of human axons that had previously been validated using DC pulses (Howells et al. 2012), and has found a tight correlation of excitability and membrane potential for hyperpolarized axons over this frequency range. This confirms the conclusions of Bostock and Baker (1988).

The relationship between changes in excitability and the underlying membrane potential has greatly assisted the interpretation of axonal excitability studies (Bostock et al. 1998). The linearity of such a relationship is not a requirement for the analysis of such data and has never been tested in these studies. However, in the present study which uses a linear systems formulation, the linearity of the relationship is crucial. The theoretical basis of such a relationship, comes from the observation that the current-voltage curves of myelinated axons are linear for short pulses, leading Bostock et al. (1991a) to argue that the current threshold is consequently proportional to the voltage threshold.

Comparison with the responses produced by DC conditioning stimuli

The 'threshold impedance' data presented in this study can be related to the threshold conductance derived from the current-threshold relationship in conventional excitability studies (Howells et al. 2012). The reciprocal of the slope of the current-threshold relationship gives the threshold impedance, albeit in response to a 200-ms square pulse (giving a period for the first harmonic of 400 ms). The fundamental frequency is thus of 2.5 Hz, comparable to the resonant frequencies for the hyperpolarized axons presented in this study. Using the model data from Howells et al. (2012), the threshold impedances would be: motor 4.06 (60%), 1.75 (0%); sensory 3.56 (60%), 1.33 (0%). These values compare favourably to the data shown in Fig. 4.

The ZAP protocol provided the opportunity to test the models developed in Howells et al. (2012) against a different stimulus paradigm, and also to test the model in the frequency domain. Without further modification, the models provided a remarkably good fit to the ZAP data (Fig. 5), providing independent verification of the dynamics of the modelled conductances of motor and sensory axons.

Factors contributing to resonance in hyperpolarized motor and sensory axons

Two mechanisms are required to generate resonance in axons. The combination of suitable low-pass and high-pass filters allows such a resonance to occur, and this is realised electrically in tuned (RLC) circuits which consist of the parallel combination of a **R**esistor, inductor (**L**) and **C**apacitor (Hutcheon and Yarom 2000). The input conductance and membrane capacitance form the necessary low-pass filter, limiting the rate at which membrane potential changes can occur in response to input stimuli according to the membrane time constant (RC). The high-pass filtering is achieved by

516 the so-called 'inductive' reactances which slowly oppose changes in membrane
517 potential.

518 **Low-frequency attenuation**

519 In human axons, the slow rectifying conductances, G_H and G_{Ks}, provide the
520 'inductive' attenuation of output responses at low frequencies. The modelling in this
521 study provided support for the view that G_{Ks} and G_H play complementary roles (Howells
522 et al. 2012). G_{Ks} contributes to the low-frequency attenuation at less-hyperpolarized
523 membrane potentials in motor axons, while G_H attenuates the low-frequency response
524 for hyperpolarization below RMP (Biel et al. 2009). The modelling demonstrated that
525 the action of I_h was confined to frequencies below ~ 3 Hz, and that I_{Ks} had a more
526 gradual attenuation across the frequencies studied. This suggests that I_{Ks} also
527 contributes to the high-frequency attenuation of responses by augmenting the input
528 conductance (Hutcheon and Yarom 2000).

529 **High-frequency attenuation**

530 As previously discussed, the low-pass filtering of the membrane is due to the
531 parallel combination of the nodal capacitance and input conductance. As the membrane
532 capacitance is essentially constant, the low-pass filtering is governed by changes in the
533 input conductance which itself is the parallel combination of all open channels. For the
534 axons in the present study these are predominantly G_{Lk} and G_{Ks}. G_{Lk} increases and G_{Ks}
535 decreases with hyperpolarization from rest, providing a complementary control over the
536 input conductance and thereby the low-pass filtering of the membrane (Hutcheon and
537 Yarom 2000).

538 **Amplifiers and suppressors of resonance**

In contrast to the effects of I_{Lk} on the frequency response, I_{NaP} potentiates the response of human axons to oscillatory input currents. This confirms previous studies which have examined the effect of TTX on the frequency-response curve and have shown a significant decrease in the magnitude of the resonant peak, particularly at depolarized membrane potentials (Gutfreund et al. 1995; Hu et al. 2002; Hutcheon et al. 1996; Wang et al. 2006).

Differences between motor and sensory axons

It is tempting to attribute the observed differences in the frequency response of motor and sensory axons to differences in their resting membrane potentials. Figure 9 shows that the responses of the motor model do indeed approximate those of the sensory model more closely when it is depolarized by an amount equivalent to a 3-mV depolarization of RMP (compare discrepancy between the blue and red traces in the lower plot to the black and red traces in the middle plot). On closer examination however, the low-frequency attenuation for the hyperpolarized axons is not improved by depolarization, and there is a suggestion that at higher frequencies depolarization attenuates the responses of motor axons further. We therefore suggest that, while a difference in membrane potential may be a major contributor to the difference in the responses of sensory and motor axons, other factors are important.

The key differences between the motor and sensory models (reported by Howells et al. 2012) are likely to contribute to the differential frequency responses. These differences are a near-halving of nodal G_{Ks}, up-modulation of I_h and an increase in I_{NaP} (the latter secondary to depolarization of resting membrane potential) in sensory axons.

Application of this technique to resonance under other conditions

563 The present study has examined the mechanisms underlying low-frequency
564 resonance of hyperpolarized human axons, but this *in vivo* technique could also be used
565 to study the interactions of other voltage-gated ion channels using different frequencies
566 and with different levels of polarization. There was evidence in the present study that
567 resonance may occur with *depolarization*: in some subjects the balancing anti-stimulus
568 excited axons at higher frequencies (not shown). Such activity is comparable to the M-
569 resonance observed in rat hippocampal pyramidal cells (Hu et al. 2002), and it is likely
570 that the rhythmic spontaneous activity recorded from *demyelinated* rat spinal root axons
571 would also have demonstrated a resonant peak in the frequency domain (Baker and
572 Bostock 1992).

573 One extension of this study could involve studying resonant behavior during
574 depolarization, and this might have more relevance to ectopic activity in demyelinating
575 neuropathies.

576 **Functional consequences**

577 The primary motivation for studying the low-frequency resonance of human
578 axons in this study was to resolve the contributions of I_h, I_{Ks} and I_{Lk} to excitability.
579 Conventional excitability studies using steady DC currents such as threshold
580 electrotonus can provide only limited insight into the relative contributions of the
581 activity of different channels at different membrane potentials. The fact that a
582 low-frequency resonance was found in healthy axons of peripheral nerve raises the
583 questions: "Are there functional consequences of this resonance in healthy axons of
584 peripheral nerve", or "is it merely an expected consequence of the time-domain
585 properties of ion channels"?

586 The low-frequency response was not substantially different in the
587 hyperpolarized axons of motor and sensory nerve. Considering the different functional
588 requirements of these axons, perhaps the basis of such a resonance is common and
589 relates to the activation of I_h during activity-dependent hyperpolarization.
590 While it might be attractive to relate the resonance explored here to the ectopic
591 firing of peripheral axons, ectopic discharge rates are too high, at least in sensory axons
592 (Burke and Applegate 1989; Culp et al. 1982; Ochoa and Torebjörk 1980). There is
593 thus little reason to argue for an important role for I_h in ectopic activity in large
594 myelinated axons. However, in contrast to central neurons (and the heart),
595 rhythmogenesis is not a desirable property of peripheral axons. Monnier (1952)
596 observed that stability in normal peripheral axons was achieved by significant damping
597 of resonance, which he called "pararesonance". The pattern of resonance in his work is
598 not unlike the resonance seen in the current study.
599

References

Baker M, and Bostock H. Ectopic activity in demyelinated spinal root axons of the rat. *J Physiol* 451: 539-552, 1992.

Barrett EF, and Barrett JN. Intracellular recording from vertebrate myelinated axons: mechanism of the depolarizing afterpotential. *J Physiol* 323: 117-144, 1982.

Biel M, Wahl-Schott C, Michalakis S, and Zong X. Hyperpolarization-activated cation channels: from genes to function. *Physiol Rev* 89: 847-885, 2009.

Boërio D, Bostock H, Spescha R, and Z'Graggen WJ. Potassium and the excitability properties of normal human motor axons in vivo. *PLoS One* 9: e98262, 2014.

Bostock H, and Baker M. Evidence for two types of potassium channel in human motor axons in vivo. *Brain Res* 462: 354-358, 1988.

Bostock H, Baker M, Grafe P, and Reid G. Changes in excitability and accommodation of human motor axons following brief periods of ischaemia. *J Physiol* 441: 513-535, 1991a.

Bostock H, Baker M, and Reid G. Changes in excitability of human motor axons underlying post-ischaemic fasciculations: evidence for two stable states. *J Physiol* 441: 537-557, 1991b.

Bostock H, Burke D, and Hales JP. Differences in behaviour of sensory and motor axons following release of ischaemia. *Brain* 117: 225-234, 1994.

Bostock H, Cikurel K, and Burke D. Threshold tracking techniques in the study of human peripheral nerve. *Muscle Nerve* 21: 137-158, 1998.

Burke D, and Applegate C. Paraesthesiae and hypaesthesia following prolonged high-frequency stimulation of cutaneous afferents. *Brain* 112: 913-929, 1989.

Burke D, Kiernan MC, and Bostock H. Excitability of human axons. *Clin Neurophysiol* 112: 1575-1585, 2001.

Cole KS. Rectification and inductance in the squid giant axon. *J Gen Physiol* 25: 29-51, 1941.

Cole KS, and Baker RF. Transverse impedance of the squid giant axon during current flow. *J Gen Physiol* 24: 535-549, 1941.

Cole KS, and Curtis HJ. Electric impedance of nerve and muscle. In: *Cold Spring Harbor symposia on quantitative biology*Cold Spring Harbor Laboratory Press, 1936, p. 73-89.

Culp WJ, Ochoa JL, and Torebjörk E. Ectopic impulse generation in myelinated sensory nerve fibers in man. In: *Abnormal nerves and muscles as impulse generators*, edited by Culp WJ, and Ochoa JLOxford University Press, 1982, p. 490-512.

Eduardo E, and Burke D. The optimal recording electrode configuration for compound sensory action potentials. *J Neurol Neurosurg Psychiatry* 51: 684-687, 1988.

Gabriel C. Compilation of the dielectric properties of body tissues at RF and microwave frequencies AFOSR/NL, 1996.

Gutfreund Y, Yarom Y, and Segev I. Subthreshold oscillations and resonant frequency in guinea-pig cortical neurons: physiology and modelling. *J Physiol* 483: 621-640, 1995.

Howells J, Czesnik D, Trevillion L, and Burke D. Excitability and the safety margin in human axons during hyperthermia. *J Physiol* 591: 3063-3080, 2013.

Howells J, Trevillion L, Bostock H, and Burke D. The voltage dependence of I(h) in human myelinated axons. *J Physiol* 590: 1625-1640, 2012.

Hu H, Vervaeke K, Graham LJ, and Storm JF. Complementary theta resonance filtering by two spatially segregated mechanisms in CA1 hippocampal pyramidal neurons. *J Neurosci* 29: 14472-14483, 2009.

Hu H, Vervaeke K, and Storm JF. Two forms of electrical resonance at theta frequencies, generated by M-current, h-current and persistent Na+ current in rat hippocampal pyramidal cells. *J Physiol* 545: 783-805, 2002.

Hutcheon B, Miura RM, and Puil E. Subthreshold membrane resonance in neocortical neurons. *J Neurophysiol* 76: 683-697, 1996.
Hutcheon B, and Yarom Y. Resonance, oscillation and the intrinsic frequency preferences of neurons. *Trends Neurosci* 23: 216-222, 2000.
Kiernan MC, Burke D, Andersen KV, and Bostock H. Multiple measures of axonal excitability: a new approach in clinical testing. *Muscle Nerve* 23: 399-409, 2000.
Koch C. Cable theory in neurons with active, linearized membranes. *Biol Cybern* 50: 15-33, 1984.
Krishnan AV, Lin CS-Y, Park SB, and Kiernan MC. Axonal ion channels from bench to bedside: a translational neuroscience perspective. *Prog Neurobiol* 89: 288-313, 2009.
Lin CS-Y, Kiernan MC, Burke D, and Bostock H. Assessment of nerve excitability properties in peripheral nerve disease. In: *Peripheral Nerve Diseases*, edited by Kimura J. Amsterdam: Elsevier, 2006, p. 381-403.
Lin CS-Y, Kuwabara S, Cappelen-Smith C, and Burke D. Responses of human sensory and motor axons to the release of ischaemia and to hyperpolarizing currents. *J Physiol* 541: 1025-1039, 2002.
Llinás RR. The intrinsic electrophysiological properties of mammalian neurons: insights into central nervous system function. *Science* 242: 1654-1664, 1988.
Logothetis NK, Kayser C, and Oeltermann A. In vivo measurement of cortical impedance spectrum in monkeys: implications for signal propagation. *Neuron* 55: 809-823, 2007.
Monnier AM. The damping factor as a functional criterion in nerve physiology. *Cold Spring Harb Symp Quant Biol* 17: 69-95, 1952.
Narayanan R, and Johnston D. The h channel mediates location dependence and plasticity of intrinsic phase response in rat hippocampal neurons. *J Neurosci* 28: 5846-5860, 2008.
Ochoa JL, and Torebjörk HE. Paraesthesiae from ectopic impulse generation in human sensory nerves. *Brain* 103: 835-853, 1980.
Orio P, Madrid R, de la Pena E, Parra A, Meseguer V, Bayliss DA, Belmonte C, and Viana F. Characteristics and physiological role of hyperpolarization activated currents in mouse cold thermoreceptors. *J Physiol* 587: 1961-1976, 2009.
Pike FG, Goddard RS, Suckling JM, Ganter P, Kasthuri N, and Paulsen O. Distinct frequency preferences of different types of rat hippocampal neurones in response to oscillatory input currents. *J Physiol* 529: 205-213, 2000.
Puil E, Gimbarzevsky B, and Miura RM. Quantification of membrane properties of trigeminal root ganglion neurons in guinea pigs. *J Neurophysiol* 55: 995-1016, 1986.
Puil E, Gimbarzevsky B, and Spigelman I. Primary involvement of K+ conductance in membrane resonance of trigeminal root ganglion neurons. *J Neurophysiol* 59: 77-89, 1988.
Puil E, Meiri H, and Yarom Y. Resonant behavior and frequency preferences of thalamic neurons. *J Neurophysiol* 71: 575-582, 1994.
Tomlinson S, Burke D, Hanna M, Koltzenburg M, and Bostock H. In vivo assessment of HCN channel current (I(h)) in human motor axons. *Muscle Nerve* 41: 247-256, 2010.
Wang WT, Wan YH, Zhu JL, Lei GS, Wang YY, Zhang P, and Hu SJ. Theta-frequency membrane resonance and its ionic mechanisms in rat subicular pyramidal neurons. *Neuroscience* 140: 45-55, 2006.
Zemankovics R, Kali S, Paulsen O, Freund TF, and Hajos N. Differences in subthreshold resonance of hippocampal pyramidal cells and interneurons: the role of h-current and passive membrane characteristics. *J Physiol* 588: 2109-2132, 2010.

Author contributions

All authors contributed to all aspects of the study, and have approved the final version of the manuscript.

Acknowledgements

The authors wish to thank Adelle Coster and Hans Coster for valuable discussions during the preparation of the manuscript. This research was supported by the National Health and Medical Research Council of Australia.

Disclosures

H.B. receives royalties from the sales of the QTRAC software. J.H. and D.B. have no conflicts of interest to report.

Tables

Table 1. Spectral parameters

Subject	$Z_{0.5Hz}$	Z_{max}	Q	f_{max}
		Motor 0%		
1	1.1 [1.6]	2.3 [2.2]	2.1 [1.4]	2.0 [7.2]
2	1.5 [1.5]	2.4 [2.1]	1.6 [1.4]	7.5 [6.2]
3	1.2 [1.2]	2.0 [1.9]	1.7 [1.6]	3.5 [5.7]
4	1.2 [1.5]	2.5 [2.2]	2.1 [1.4]	4.5 [4.9]
5	1.5 [1.4]	2.5 [2.2]	1.7 [1.5]	3.3 [5.4]
6	1.3 [1.3]	2.7 [2.3]	2.0 [1.8]	7.3 [6.2]
Mean	**1.3 [1.4]**	**2.4 [2.1]**	**1.9 [1.5]**	**4.7 [5.9]**
		Motor 60%		
1	1.4 [1.7]	3.9 [3.9]	2.8 [2.3]	2.75 [2.4]
2	1.7 [1.4]	3.7 [3.6]	2.2 [2.6]	2.5 [2.5]
3	2.0 [1.8]	4.4 [4.1]	2.2 [2.3]	2.25 [2.3]
4	3.6 [2.9]	5.3 [4.7]	1.5 [1.6]	2.0 [1.8]
5	5.0 [3.7]	5.8 [5.2]	1.2 [1.4]	2.0 [1.7]
6	4.1 [3.0]	6.0 [5.5]	1.5 [1.9]	2.25 [2.0]
Mean	**3.0 [2.4]**	**4.8 [4.5]**	**1.9 [2.0]**	**2.3 [2.1]**
		Sensory 0%		
1	0.5 [1.1]	1.8 [1.5]	3.7 [1.3]	9.25 [7.5]
2	0.8 [1.1]	2.3 [1.9]	2.9 [1.7]	3.5 [5.7]
3	1.1 [1.0]	2.1 [1.7]	1.9 [1.6]	4.75 [5.2]
4	0.9 [1.4]	2.1 [1.8]	2.2 [1.3]	2.0 [6.5]
5	1.4 [1.3]	2.2 [1.7]	1.6 [1.3]	4.8 [6.8]
6	0.8 [1.2]	1.8 [1.7]	2.2 [1.4]	9.25 [7.2]
Mean	**0.9 [1.2]**	**2.1 [1.7]**	**2.4 [1.4]**	**5.6 [6.5]**
		Sensory 60%		
1	1.9 [1.9]	3.6 [3.2]	1.9 [1.7]	4.25 [3.0]
2	0.8 [1.3]	3.9 [3.3]	4.6 [2.6]	3.5 [2.7]
3	2.6 [2.2]	5.1 [4.5]	1.9 [2.0]	2.0 [2.2]
4	2.6 [2.3]	4.7 [4.3]	1.8 [1.9]	2.0 [2.4]
5	2.3 [2.6]	5.2 [4.4]	2.3 [1.7]	2.0 [1.8]
6	2.9 [2.4]	4.0 [3.5]	1.4 [1.5]	2.0 [2.8]
Mean	**2.2 [2.1]**	**4.4 [3.9]**	**2.3 [1.9]**	**2.6 [2.5]**

Derived parameters summarizing the frequency response of motor axons and sensory axons at RMP (0%) and with a 60% hyperpolarization. Bracketed values were calculated after first smoothing the data with a Pearson Type IV function.

714 **Table 2. Spectral parameters derived from modelled data**

	$Z_{0.5Hz}$	Z_{max}	Q	f_{max}
Motor 0%	1.2 [1.4]	2.4 [2.3]	1.9 [1.6]	4.5 [4.9]
Motor 60%	2.9 [2.6]	4.9 [4.6]	1.7 [1.8]	2.3 [2.1]
Sensory 0%	0.9 [1.1]	1.8 [1.8]	1.9 [1.6]	9.3 [6.5]
Sensory 60%	2.3 [2.2]	4.1 [3.9]	1.8 [1.8]	2.0 [2.6]

715

716 Bracketed values were calculated after first smoothing the data with a Pearson Type IV function.

717

Figures

Figure 1. Measures of impedance and 'threshold impedance' in a model of human motor axons. **a.** DC to 16Hz ZAP stimulus (10% of threshold) applied at RMP (red) and with 60% hyperpolarization (blue). **b,e,h.** Response, electrical impedance magnitude and phase measured using membrane potential. **c,f,i.** Response, 'impedance' magnitude and phase measured using threshold change. **d,g.** Impedance magnitude and phase difference measured using membrane potential and individual sinewave stimuli at frequencies of 0.5, 0.75, 1, 1.5, 2, 3, 4, 6, 8, 10, 12 and 16 Hz.

Figure 2. Correlation of electrical impedance and 'threshold impedance' measures in the model. **a.** Correlation of excitability and membrane potential in response to the same input stimulus (data from Fig. 1b,c) **b.** Magnitude of 'threshold impedance' vs conventional electrical impedance (data from Fig. 1e,f). **c.** Phase difference between response and input measured using the threshold and membrane potential methods (data from Fig. 1 h,i). The yellow to red data points correspond to data gathered at RMP and are graded according to frequency (see scale, lower left). Similarly the green to blue data points correspond to the hyperpolarized data.

Figure 3. Comparison of Frequency Response Curves derived from 16-s and 4-s ZAPs. Blue and red traces are from 4-s ZAP stimuli at RMP and with 60% hyperpolarization. Grey traces are for the corresponding 16-s ZAP stimuli. **a.** Membrane potential change. **b.** Electrical impedance magnitude (linear regression of 16-s vs 4-s data: $y=0.98*x -0.001$, $R^2=0.94$; i.e. close to the line of identity). **c.** Phase difference between membrane potential and stimulus current (linear regression: $y=1.10*x+0.053$, $R^2=0.86$).

Figure 4. Excitability changes in response to ZAP conditioning. *Upper Row:* Superimposed responses of the six subjects at RMP (red) and with hyperpolarization (blue) in motor and

sensory axons. *Middle Row:* Mean (± SEM) magnitude of threshold impedance versus frequency (n=6). *Bottom Row:* Mean (± SEM) phase difference between response and input stimulus.

Figure 5. Comparison of modelled and observed data.

Observed data (mean [solid lines] ± SEM [dashed lines] for RMP [red] and 60% hyperpolarization [blue]) and modelled data (black lines). *Top Row*, Response to input ZAP at RMP and with 60% hyperpolarization. *Bottom Row*, Magnitude of 'threshold impedance' $|'Z_{threshold}'|$ versus frequency for the axons at RMP and with hyperpolarization.

Figure 6. Voltage dependence of the frequency response in the model motor axon.

a Threshold electrotonic responses at RMP (0%, red) and for 30 (green), 60 (blue) and 90% (cyan) hyperpolarizations. **b**. Response to ZAP conditioning superimposed on the hyperpolarizations in *A*. *c.* Magnitude of the threshold impedance calculated from the responses in *b.* **d**. Phase of the threshold impedance, corresponding to the difference between response and input stimulus.

Figure 7. Ion channels contributing to the low-frequency resonance. Membrane potential (EN, top), currents (I, middle) and channel open fractions (bottom) for motor axons in response to the ZAP protocol modelled at RMP (left column), and with -60% hyperpolarization (right column).

Figure 8. Sensitivity of frequency response to key currents. Thin lines correspond to the unaltered model (same as Fig 1e). The dotted lines correspond to the removal of a conductance, and the thicker lines are with the same conductance doubled. The red and blue lines are modelled at RMP and with 60% hyperpolarization, respectively. **a.** G_H (maximal conductance of I_h). **b.** G_{Ks} (maximal conductance of slow K^+ channels). **c.** G_{Lk} (maximal conductance of ohmic 'leak' channels). **d.** P_{NaP} (fraction of Na^+ channels operarting in a

persistent mode). Note: RMP and hyperpolarization were clamped for each conductance alteration to maintain the same average potential as in the unaltered data.

Figure 9. Do sensory axons behave as relatively depolarized motor axons?

Observed excitability responses (mean ± SEM) to ZAP function (**a.**) and frequency-response curves (**b.**) for motor (black) and sensory (red) axons at RMP and with a 60% hyperpolarization. Modelled excitability (**c.**) and frequency-response (**d.**): motor model (black), sensory model (red). Depolarised motor model (blue) and sensory model (red) excitability (**e.**) and frequency response (**f.**).

Appendix

Modelling equations and parameters

Membrane potential: (asterisks denote internodal parameters)

$$\frac{dE}{dt} = -\frac{I_{Na} + I_{Kf} + I_{Ks} + I_{Lk} + I_{pump} + I_{external} + I_{BB}}{C_n + C_{myelin}}$$

$$\frac{dE^*}{dt} = -\frac{I_{Kf^*} + I_{Ks^*} + I_h + I_{pump^*} + I_{Lk^*} - I_{BB} - C_{myelin}\frac{dE}{dt}}{C_{ax}}$$

Capacitance:

$$C_n = 1.4 \qquad C_{myelin} = 1.55 \qquad C_{ax} = 327\ pF$$

Ion concentrations:

$$[Na]_i = 9 \qquad [Na]_o = 144.2 \qquad [K]_i = 155 \qquad [K]_o = 4.5\ mM$$

Sodium current:

$$I_{Na} = P_{Na}(m^3 h) z(Na) \qquad I_{NaP} = P_{Na}\left(\frac{P_{NaP}}{100} m_p^3\right) z(Na)$$

$$z(Na) = \frac{EF^2}{RT}\left(\frac{Sel_{Na}\left\{[Na]_o - [Na]_i \exp\left(\frac{EF}{RT}\right)\right\} + (1 - Sel_{Na})\left\{[K]_o - [K]_i \exp\left(\frac{EF}{RT}\right)\right\}}{1 - \exp\left(\frac{EF}{RT}\right)}\right)$$

Fast potassium current:

$$I_{Kf} = G_{Kf} n^4 (E - E_{Kf}) \qquad I_{Kf^*} = G_{Kf^*} n^{*4} (E^* - E_{Kf})$$

Slow potassium current:

$$I_{Ks} = G_{Ks} s (E - E_{Ks}) \qquad I_{Ks^*} = G_{Ks^*} s^* (E^* - E_{Ks})$$

Leak current:

$$I_{Lk} = G_{Lk}(E - E_r) \qquad I_{Lk^*} = G_{Lk^*}(E^* - E_r^*)$$

Barrett-Barrett current:

$$I_{BB} = G_{BB}(E - E^*)$$

Current through HCN channels:

$$I_h = G_h q (E^* - E_h)$$

Equilibrium potentials:

$$E_x = \frac{RT}{F} \ln\left(\frac{[K]_o + Sel_x[Na]_o - Sel_x[K]_o}{[K]_i + Sel_x[Na]_i - Sel_x[K]_i}\right) \text{ for } x = K_f, K_s, h$$

$$Sel_{Na} = 0.9, \quad Sel_{Kf}, Sel_{Ks} = 0, \quad Sel_h = 0.097$$

Voltage dependence and kinetics:

$$\frac{dm}{dt} = \alpha_m(1 - m) - \beta_m m \qquad \text{and similarly for } m_p, h, n, s, n^*, s^*, q$$

$$\alpha_m, \alpha_{m_p}, \alpha_n, \alpha_s = \frac{A(E - B)}{1 - \exp((\mathrm{B} - \mathrm{E})/\mathrm{C})} \qquad \alpha_h, \beta_m, \beta_{m_p}, \beta_n, \beta_s = \frac{A(B - E)}{1 - \exp\left(\frac{E - B}{C}\right)}$$

$$\beta_h = \frac{A}{1 + \exp\left(\frac{B - E}{C}\right)} \qquad \alpha_q = A \exp\left(\frac{E - B}{C}\right)$$

$$\beta_q = A/\exp((E - B)/C)$$

	A (ms^{-1}, at 36°C)	*Q10*	*B (mV)*	*C (mV)*
α_m	6.54 (6.25)	2.2	-18.5 (-18.3)	10.3
β_m	0.302 (0.289)		-22.8 (-22.6)	9.16
α_{m_p}	3.27 (3.13)		-36.5 (-36.3)	10.3
β_{m_p}	0.151 (0.145)		-40.8 (-40.6)	9.16
α_h	0.126 (0.153)	2.9	-115.1 (-113.8)	15.6 (11.9)
β_h	8.60 (10.5)		-32.9 (-31.6)	19.0 (14.5)
α_n	0.0221	3.0	-90.8	7.7
β_n	0.0393		-73.6	7.35
α_s	0.00563		-23.5	12.7
β_s	0.00341		-91.1	11.7
α_q, β_q	0.00522		-107.3 (-94.2)	-12.2

Sensory parameters (bracketed values)

Maximum conductances and permeabilities:

Parameter	*Description*	*Motor*	*Sensory*
PNaN (cm^3s^{-1}x 10^{-9})	Permeability of Na^+ channels at the node	4.35	4.35
PNaP% (%)	% of Na^+ channels that are persistent	1.07	1.07
GKsN (nS)	Max. conductance of slow K^+ channels at the node	56.7	29.1
GKsI (nS)	Max. conductance of slow K^+ channels at the internode	0.57	1.74
GKfN (nS)	Max. conductance of fast K^+ channels at the node	18.2	19.4
GKfI (nS)	Max. conductance of fast K^+ channels at the internode	207	205
GH (nS)	Max. conductance of I_h	2.95	4.1
GLkN (nS)	Leak conductance at the node	1.97	1.69
GLkI (nS)	Leak conductance at the internode	4	3.65
GBB (nS)	Barrett-Barrett conductance	35.9	40.3

Resting membrane potential:

EIR (mV) (I_{pump})	Internodal resting membrane potential *(internodal pump current; nA)*	-84.6 *(-7.86 x 10^{-3})*	-81.3 *(-4.3 x 10^{-3})*
ENR (mV) (I_{pump*})	Nodal resting membrane potential *(nodal pump current; nA)*	-84.4 *(-3.33 x 10^{-2})*	-80.3 *(-5.44 x 10^{-2})*

Figures

Figure 1. Measures of impedance and 'threshold impedance' in a model of human motor axons. a. DC to 16Hz ZAP stimulus (10% of threshold) applied at RMP (red) and with 60% hyperpolarization (blue). **b,e,h.** Response, electrical impedance magnitude and phase measured using membrane potential. **c,f,i.** Response, 'impedance' magnitude and phase measured using threshold change. **d,g.** Impedance magnitude and phase difference measured using membrane potential and individual sinewave stimuli at frequencies of 0.5, 0.75, 1, 1.5, 2, 3, 4, 6, 8, 10, 12 and 16 Hz.

Figure 2. Correlation of electrical impedance and 'threshold impedance' measures in the model. a. Correlation of excitability and membrane potential in response to the same input stimulus (data from Fig. 1b,c) **b.** Magnitude of 'threshold impedance' vs conventional electrical impedance (data from Fig. 1e,f). **c.** Phase difference between response and input measured using the threshold and membrane potential methods (data from Fig. 1 h,i). The yellow to red data points correspond to data gathered at RMP and are graded according to frequency (see scale, lower left). Similarly the green to blue data points correspond to the hyperpolarized data.

Figure 3. Comparison of Frequency Response Curves derived from 16-s and 4-s ZAPs. Blue and red traces are from 4-s ZAP stimuli at RMP and with 60% hyperpolarization. Grey traces are for the corresponding 16-s ZAP stimuli. **a.** Membrane potential change. **b.** Electrical impedance magnitude (linear regression of 16-s vs 4-s data: $y=0.98*x -0.001$, $R^2=0.94$; i.e. close to the line of identity). **c.** Phase difference between membrane potential and stimulus current (linear regression: $y=1.10*x+0.053$, $R^2=0.86$).

Figure 4. Excitability changes in response to ZAP conditioning. *Upper Row:* Superimposed responses of the six subjects at RMP (red) and with hyperpolarization (blue) in motor and sensory axons. *Middle Row:* Mean (± SEM) magnitude of threshold impedance versus frequency (n=6). *Bottom Row:* Mean (± SEM) phase difference between response and input stimulus.

Figure 5. Comparison of modelled and observed data.

Observed data (mean [solid lines] ± SEM [dashed lines] for RMP [red] and 60% hyperpolarization [blue]) and modelled data (black lines). *Top Row*, Response to input ZAP at RMP and with 60% hyperpolarization. *Bottom Row*, Magnitude of 'threshold impedance' $|'Z_{threshold}'|$ versus frequency for the axons at RMP and with hyperpolarization.

Figure 6. Voltage dependence of the frequency response in the model motor axon.

a Threshold electrotonic responses at RMP (0%, red) and for 30 (green), 60 (blue) and 90% (cyan) hyperpolarizations. **b**. Response to ZAP conditioning superimposed on the hyperpolarizations in *A*. *c.* Magnitude of the threshold impedance calculated from the responses in *b.* **d**. Phase of the threshold impedance, corresponding to the difference between response and input stimulus.

Figure 7. Ion channels contributing to the low-frequency resonance. Membrane potential (EN, top), currents (I, middle) and channel open fractions (bottom) for motor axons in response to the ZAP protocol modelled at RMP (left column), and with -60% hyperpolarization (right column).

Figure 8. Sensitivity of frequency response to key currents. Thin lines correspond to the unaltered model (same as Fig 1e). The dotted lines correspond to the removal of a conductance, and the thicker lines are with the same conductance doubled. The red and blue lines are modelled at RMP and with 60% hyperpolarization, respectively. **a.** G_H (maximal

conductance of I_h). **b.** G_{Ks} (maximal conductance of slow K^+ channels). **c.** G_{Lk} (maximal conductance of ohmic 'leak' channels). **d.** P_{NaP} (fraction of Na^+ channels operarting in a persistent mode). Note: RMP and hyperpolarization were clamped for each conductance alteration to maintain the same average potential as in the unaltered data.

Figure 9. Do sensory axons behave as relatively depolarized motor axons?

Observed excitability responses (mean ± SEM) to ZAP function (**a.**) and frequency-response curves (**b.**) for motor (black) and sensory (red) axons at RMP and with a 60% hyperpolarization. Modelled excitability (**c.**) and frequency-response (**d.**): motor model (black), sensory model (red). Depolarised motor model (blue) and sensory model (red) excitability (**e.**) and frequency response (**f.**).

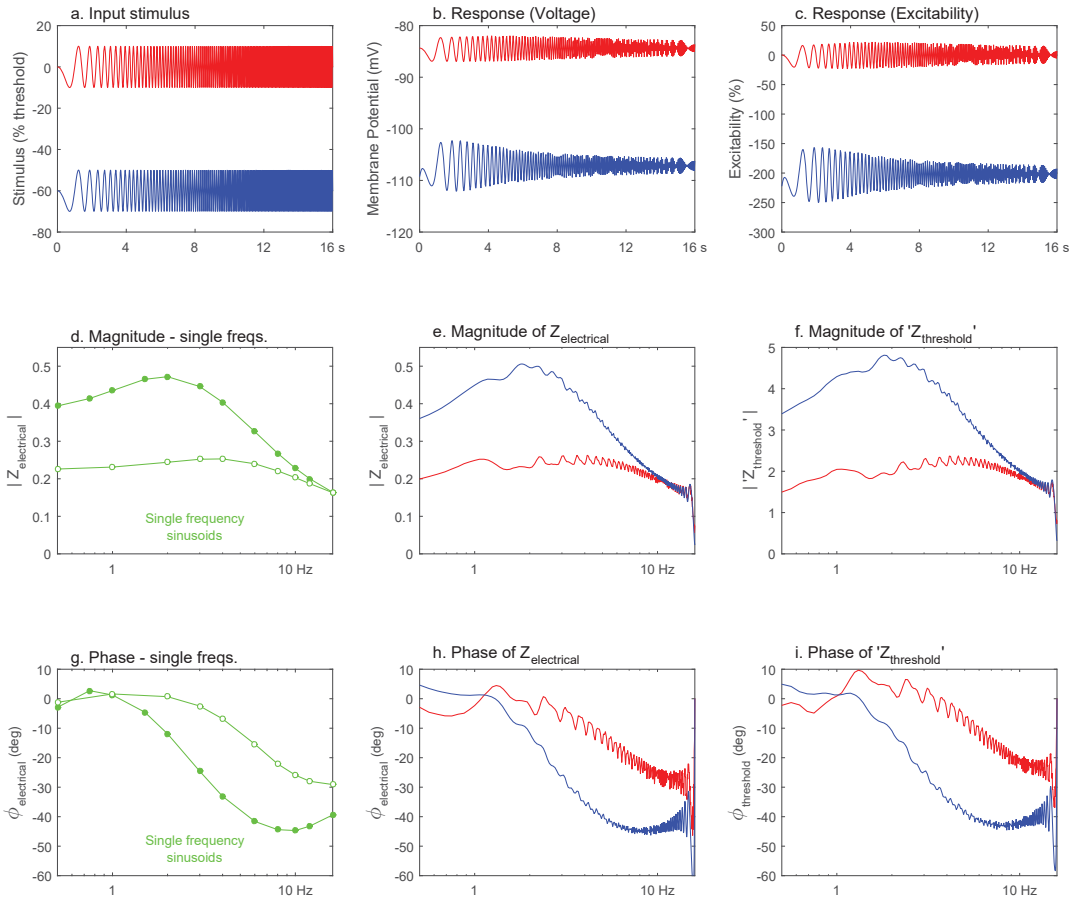
a. Input stimulus
Stimulus (% threshold)
b. Response (Voltage)
Membrane Potential (mV)
c. Response (Excitability)
Excitability (%)
d. Magnitude - single freqs.
| Z electrical |
Single frequency sinusoids
e. Magnitude of Z electrical
f. Magnitude of 'Z threshold'
g. Phase - single freqs.
h. Phase of Z electrical
i. Phase of 'Z threshold'
16 s
10 Hz

Figure 1.

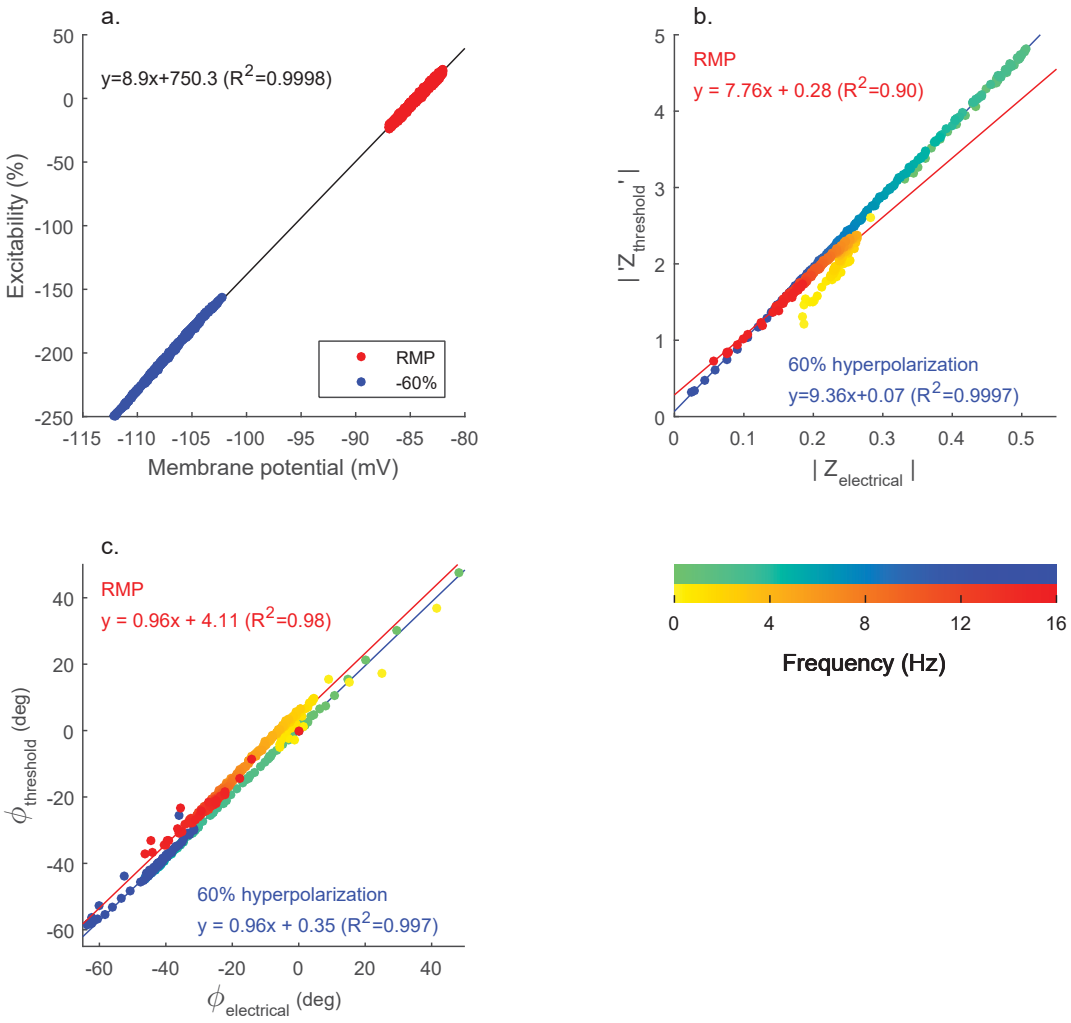
a.
y=8.9x+750.3 (R2=0.9998)
RMP
-60%
Excitability (%)
Membrane potential (mV)
b.
RMP
y = 7.76x + 0.28 (R2=0.90)
60% hyperpolarization
y=9.36x+0.07 (R2=0.9997)
| 'Zthreshold ' |
| Zelectrical |
Frequency (Hz)
c.
RMP
y = 0.96x + 4.11 (R2=0.98)
60% hyperpolarization
y = 0.96x + 0.35 (R2=0.997)
ϕthreshold (deg)
ϕelectrical (deg)

Figure 2.

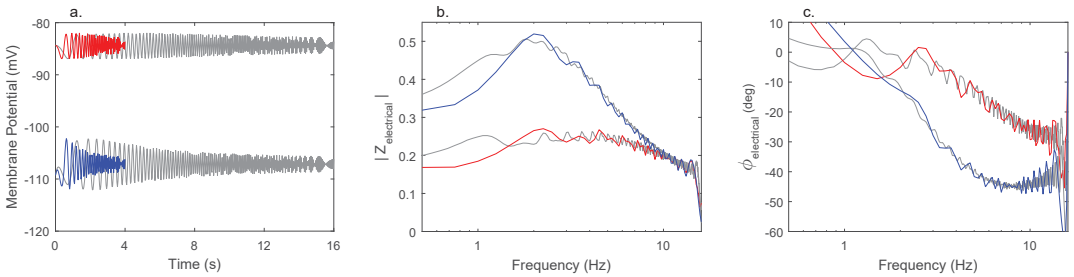
a.
b.
c.
Membrane Potential (mV)
-80
-90
-100
-110
-120
0
4
8
12
16
Time (s)
$|Z_{electrical}|$
0.5
0.4
0.3
0.2
0.1
0
1
10
Frequency (Hz)
$\phi_{electrical}$ (deg)
10
0
-10
-20
-30
-40
-50
-60
1
10
Frequency (Hz)

Figure 3.

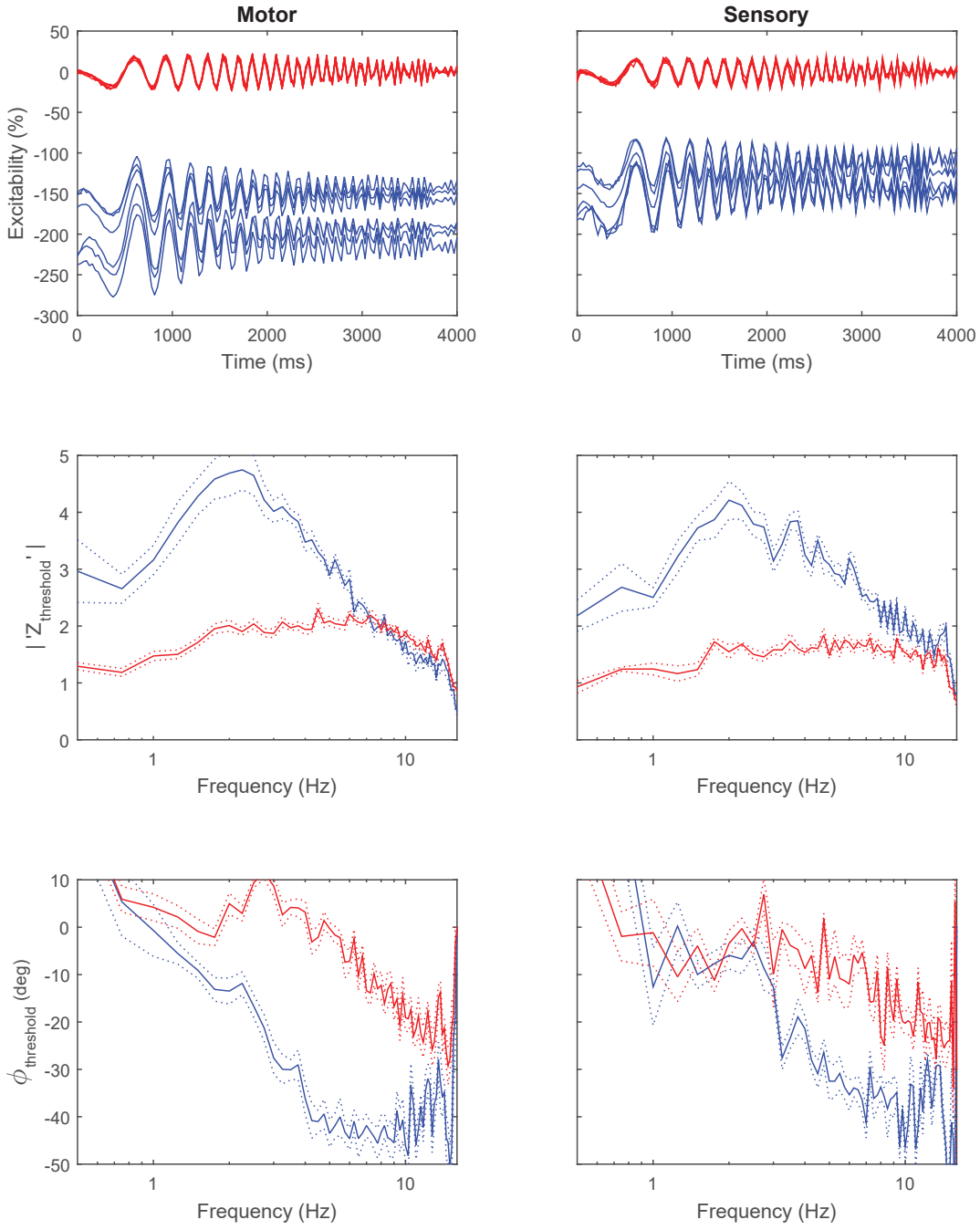
Motor
Sensory
Excitability (%)
Time (ms)
Frequency (Hz)
$|'Z_{threshold}'|$
$\phi_{threshold}$ (deg)

Figure 4.

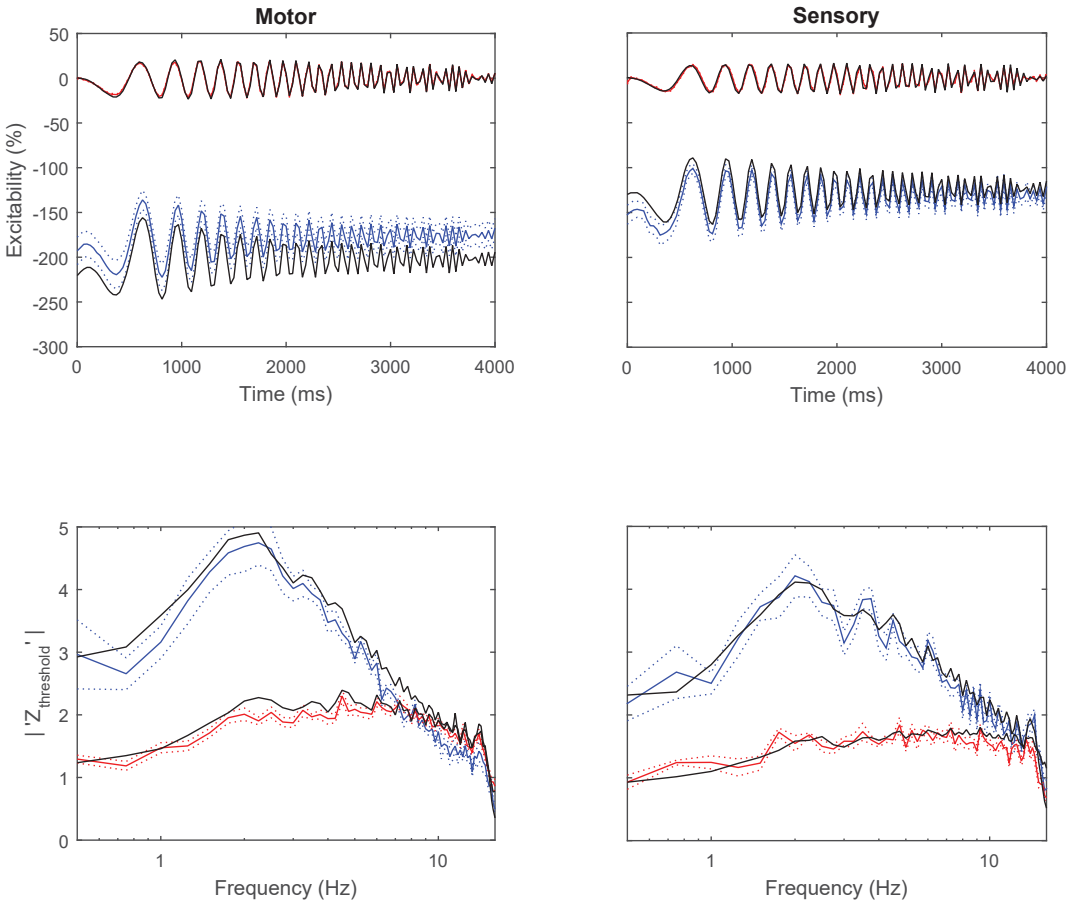
Motor
Sensory
Excitability (%)
50
0
-50
-100
-150
-200
-250
-300
0
1000
2000
3000
4000
Time (ms)
| Z'threshold |
5
4
3
2
1
0
1
10
Frequency (Hz)

Figure 5.

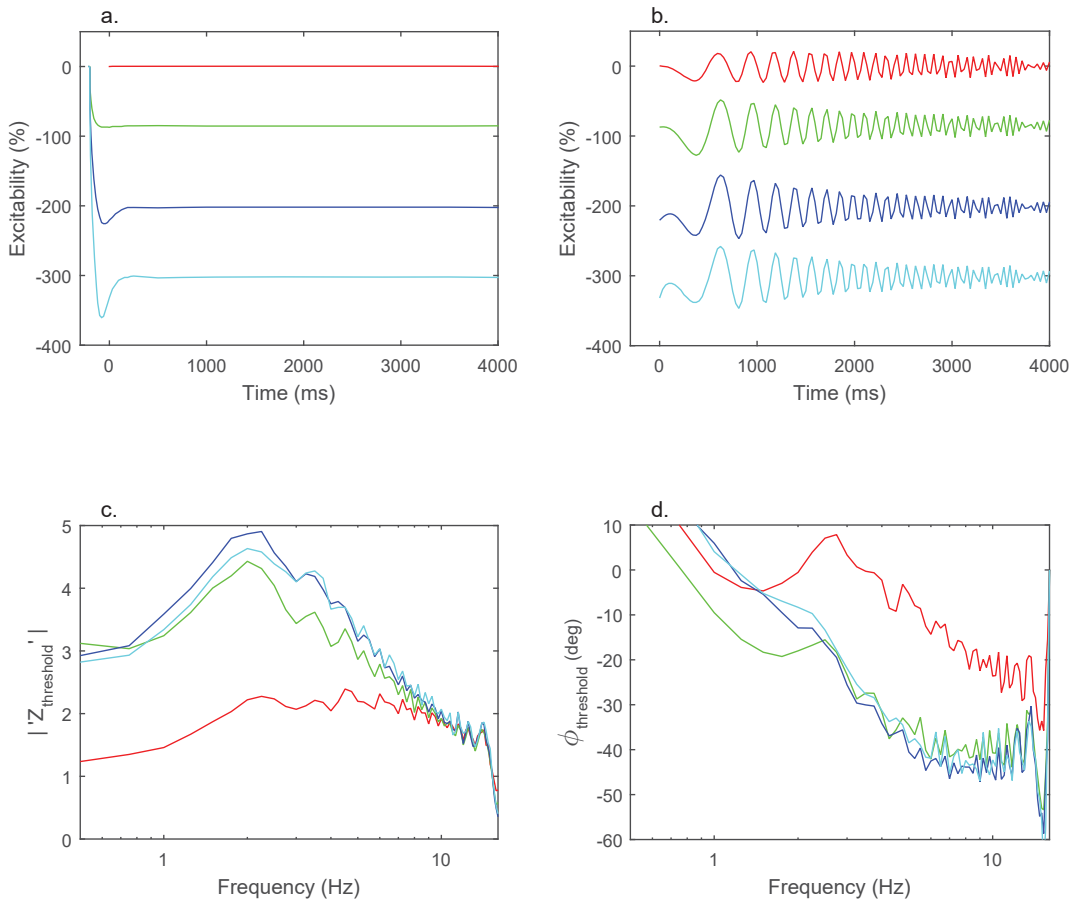
a.
b.
c.
d.
Excitability (%)
Time (ms)
Frequency (Hz)
$|Z'_{threshold}|$
$\phi_{threshold}$ (deg)

Figure 6.

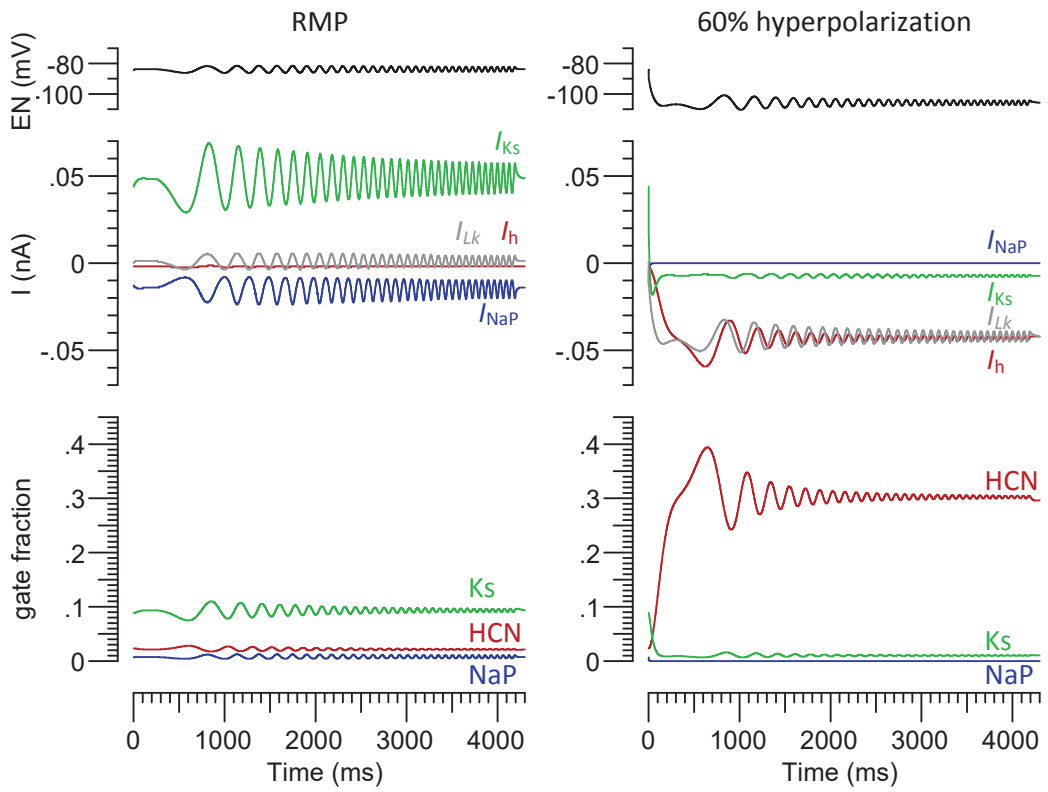
RMP
60% hyperpolarization
EN (mV)
-80
-100
I (nA)
.05
0
-.05
I_{Ks}
I_{Lk}
I_h
I_{NaP}
gate fraction
.4
.3
.2
.1
0
Ks
HCN
NaP
0
1000
2000
3000
4000
Time (ms)

Figure 7.

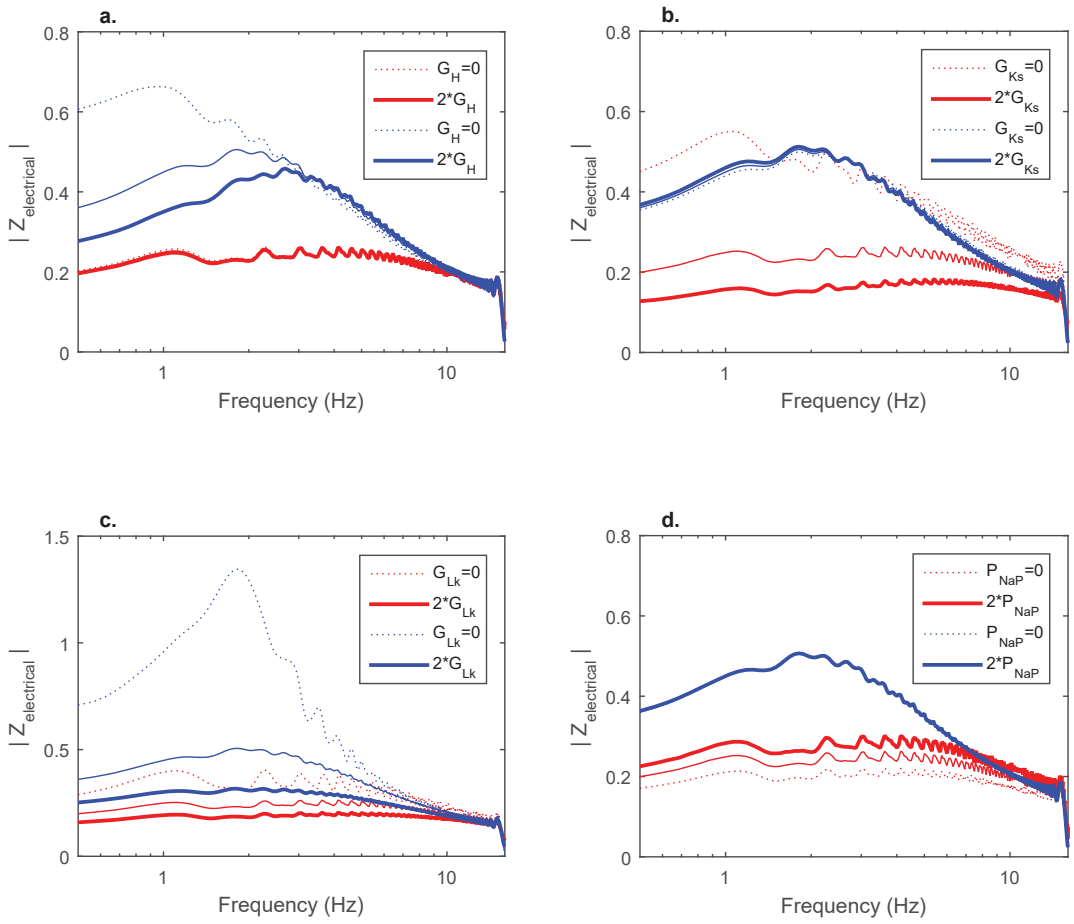
a.
b.
c.
d.
| Z electrical |
Frequency (Hz)
G H =0
2*G H
G Ks =0
2*G Ks
G Lk =0
2*G Lk
P NaP =0
2*P NaP

Figure 8.

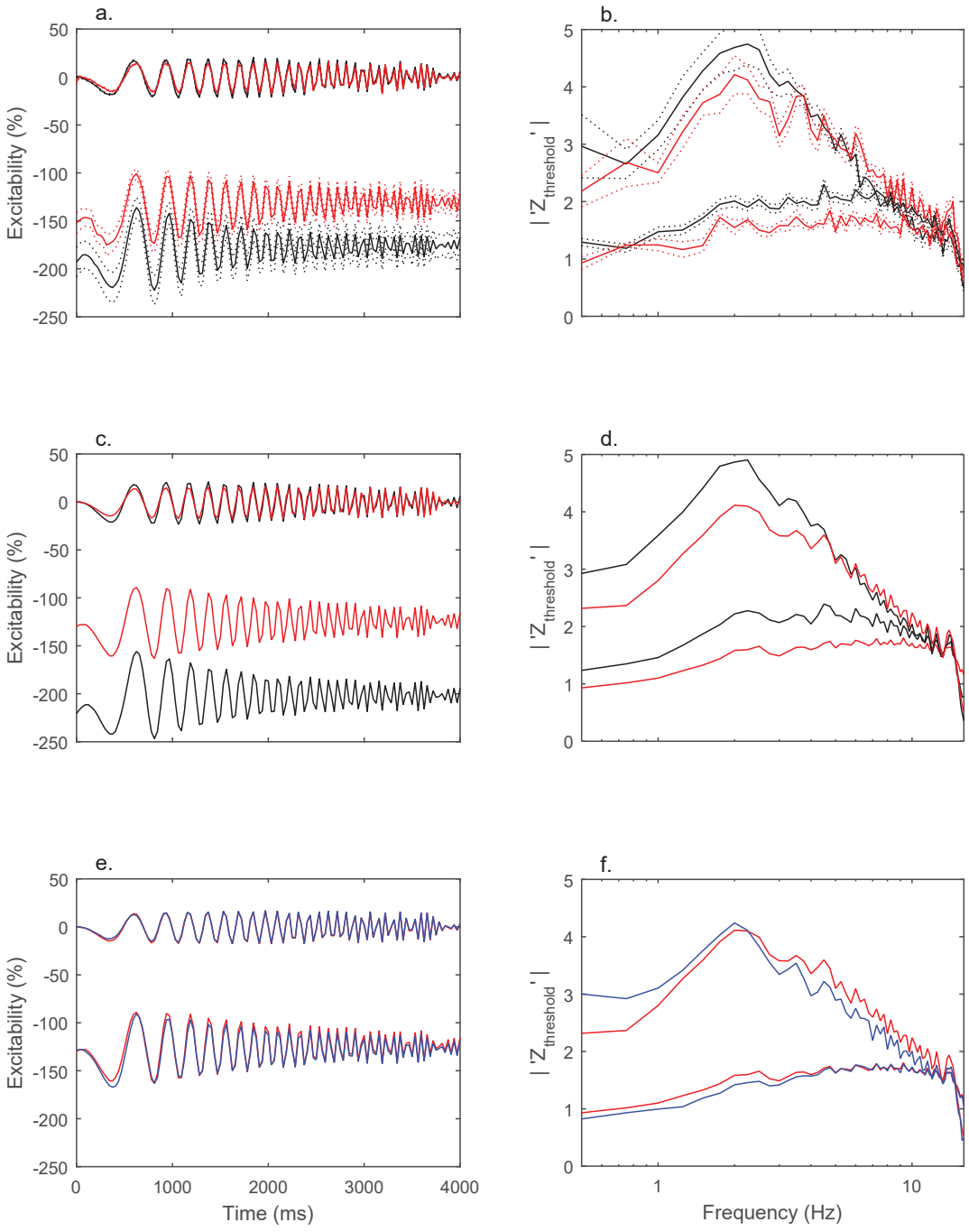
a.
b.
c.
d.
e.
f.
Excitability (%)
50
0
-50
-100
-150
-200
-250
$|'Z_{threshold}'|$
5
4
3
2
1
0
0
1000
2000
3000
4000
Time (ms)
1
10
Frequency (Hz)

Figure 9.